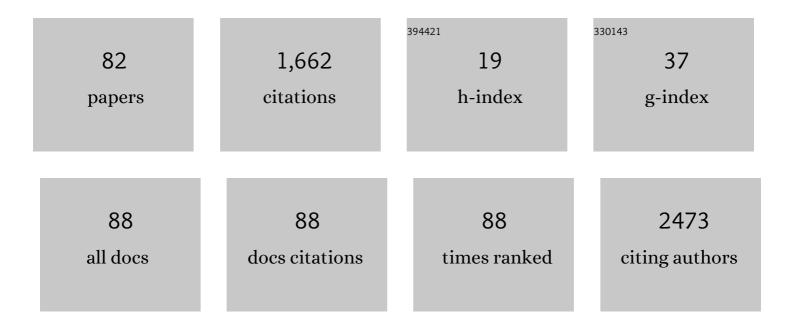
Bing Hu

List of Publications by Year in descending order

Source: https://exaly.com/author-pdf/3385/publications.pdf Version: 2024-02-01



RINC HU

#	Article	IF	CITATIONS
1	2D antimonene-integrated composite nanomedicine for augmented low-temperature photonic tumor hyperthermia by reversing cell thermoresistance. Bioactive Materials, 2022, 10, 295-305.	15.6	16
2	Failure mode effect and criticality analysis of ultrasound device by classification tracking. BMC Health Services Research, 2022, 22, 429.	2.2	2
3	Prussian blue nanozyme-mediated nanoscavenger ameliorates acute pancreatitis via inhibiting TLRs/NF-κB signaling pathway. Theranostics, 2021, 11, 3213-3228.	10.0	58
4	Lowâ€frequency ultrasound combined with microbubbles improves gene transfection in prostate cancer cells in vitro and in vivo. Asia-Pacific Journal of Clinical Oncology, 2021, , .	1.1	5
5	Monitoring radiofrequency therapyâ€induced tumor cell dissemination by in vivo flow cytometry. Cytometry Part A: the Journal of the International Society for Analytical Cytology, 2021, 99, 593-600.	1.5	2
6	Ultrasound-assisted C3F8-filled PLGA nanobubbles for enhanced FGF21 delivery and improved prophylactic treatment of diabetic cardiomyopathy. Acta Biomaterialia, 2021, 130, 395-408.	8.3	14
7	Biodegradable cascade nanocatalysts enable tumor-microenvironment remodeling for controllable CO release and targeted/synergistic cancer nanotherapy. Biomaterials, 2021, 276, 121001.	11.4	35
8	Role of "Stiff Rim―sign obtained by shear wave elastography in diagnosis and guiding therapy of breast cancer. International Journal of Medical Sciences, 2021, 18, 3615-3623.	2.5	6
9	The Design and Rationale of a Multicentre Randomised Controlled Trial Comparing Transperineal Percutaneous Laser Ablation With Transurethral Resection of the Prostate for Treating Benign Prostatic Hyperplasia. Frontiers in Surgery, 2021, 8, 755957.	1.4	11
10	Neutrophil-mediated clinical nanodrug for treatment of residual tumor after focused ultrasound ablation. Journal of Nanobiotechnology, 2021, 19, 345.	9.1	10
11	Biodegradable reduce expenditure bioreactor for augmented sonodynamic therapy via regulating tumor hypoxia and inducing pro-death autophagy. Journal of Nanobiotechnology, 2021, 19, 418.	9.1	20
12	In-situ homodispersely immobilization of Ag@AgCl on chloridized g-C3N4 nanosheets as an ultrastable plasmonic photocatalyst. Chemical Engineering Journal, 2020, 384, 123259.	12.7	64
13	The value of conventional sonography and ultrasound elastography in decision-making for thyroid nodules in different categories of the Bethesda system for reporting thyroid cytopathology. Clinical Hemorheology and Microcirculation, 2020, 74, 255-266.	1.7	9
14	Hollow Magnetic Nanocatalysts Drive Starvation–Chemodynamic–Hyperthermia Synergistic Therapy for Tumor. ACS Nano, 2020, 14, 9662-9674.	14.6	103
15	Diagnosis of Subungual Glomus Tumors with 18ÂMHz Ultrasound and CDFI. Scientific Reports, 2020, 10, 17848.	3.3	12
16	Large-scale synthesis of monodisperse Prussian blue nanoparticles for cancer theranostics via an "in situ modification" strategy. International Journal of Nanomedicine, 2019, Volume 14, 271-288.	6.7	28
17	Nanozyme-mediated catalytic nanotherapy for inflammatory bowel disease. Theranostics, 2019, 9, 2843-2855.	10.0	149
18	Hollow Prussian Blue Nanozymes Drive Neuroprotection against Ischemic Stroke via Attenuating Oxidative Stress, Counteracting Inflammation, and Suppressing Cell Apoptosis. Nano Letters, 2019, 19, 2812-2823.	9.1	203

#	Article	IF	CITATIONS
19	A new radiation force balance method for measuring diverging piston source power in the frequency range 20–100â€⁻kHz: Theory and experimental verification. Ultrasonics, 2019, 97, 11-18.	3.9	0
20	Real-Time Elastography in the diagnosis of prostate cancer: a systematic review. Medical Ultrasonography, 2019, 21, 327.	0.8	3
21	Fibroblast growth factor 21 inhibition aggravates cardiac dysfunction in diabetic cardiomyopathy by improving lipid accumulation. Experimental and Therapeutic Medicine, 2018, 15, 75-84.	1.8	12
22	Preoperative Transurethral Contrastâ€Enhanced Ultrasonography in the Diagnosis of Female Urethral Diverticula. Journal of Ultrasound in Medicine, 2018, 37, 2881-2889.	1.7	9
23	Three-Dimensional Computerized Model Based on the Sonourethrogram: A Novel Technique to Evaluate Anterior Urethral Stricture. Journal of Urology, 2018, 199, 568-575.	0.4	8
24	Theoretical and experimental study of dual-fiber laser ablation for prostate cancer. PLoS ONE, 2018, 13, e0206065.	2.5	11
25	Vascular endothelial growth factor suppresses dendritic cells function of human prostate cancer. OncoTargets and Therapy, 2018, Volume 11, 1267-1274.	2.0	19
26	Application of Real-time Elastography Ultrasound in the Diagnosis of Axillary Lymph Node Metastasis in Breast Cancer Patients. Scientific Reports, 2018, 8, 10234.	3.3	19
27	Characterization and management of various renal cystic lesions by sonographic features. Journal of the Chinese Medical Association, 2018, 81, 1017-1026.	1.4	6
28	"Alternated cooling and heating" strategy enables rapid fabrication of highly-crystalline g-C3N4 nanosheets for efficient photocatalytic water purification under visible light irradiation. Carbon, 2018, 137, 19-30.	10.3	61
29	Determining "abnormal―levator hiatus distensibility using three-dimensional transperineal ultrasound in Chinese women. Frontiers of Medicine, 2018, 12, 572-579.	3.4	8
30	Ultrasound prediction of abnormal infant development in hypertensive pregnant women in the second and third trimester. Scientific Reports, 2017, 7, 40429.	3.3	4
31	Radiation force calculation of cylindrical focusing transducer and array on ray acoustics model. AIP Conference Proceedings, 2017, , .	0.4	0
32	The Characteristics of the Transitional Zone in Prostate Growth With Age. Urology, 2017, 105, 136-140.	1.0	11
33	Liver fibrosis classification based on transfer learning and FCNet for ultrasound images. IEEE Access, 2017, , 1-1.	4.2	53
34	Establishment of the U.L.T.R.A. measurement rating system for anterior urethral stricture. International Urology and Nephrology, 2017, 49, 1201-1207.	1.4	6
35	The usefulness of global left atrial strain for predicting atrial fibrillation recurrence after catheter ablation in patients with persistent and paroxysmal atrial fibrillation. Archives of Cardiovascular Diseases, 2017, 110, 447-455.	1.6	15
36	Comparative study of conventional US, contrast enhanced US and enhanced MR for the follow-up of prostatic radiofrequency ablation. Experimental and Therapeutic Medicine, 2017, 13, 3535-3542.	1.8	11

#	Article	IF	CITATIONS
37	Effect of Roux-en-Y gastric bypass on carotid intima-media thickness in Chinese obese patients with type 2 diabetes. Surgery for Obesity and Related Diseases, 2017, 13, 1530-1535.	1.2	5
38	Injectable and thermally contractible hydroxypropyl methyl cellulose/Fe3O4 for magnetic hyperthermia ablation of tumors. Biomaterials, 2017, 128, 84-93.	11.4	64
39	Association between left atrial appendage emptying velocity, N-terminal plasma brain natriuretic peptide levels, and recurrence of atrial fibrillation after catheter ablation. Journal of Interventional Cardiac Electrophysiology, 2017, 48, 343-350.	1.3	14
40	Effect of low-frequency low-intensity ultrasound with microbubbles on prostate cancer hypoxia. Tumor Biology, 2017, 39, 101042831771927.	1.8	15
41	Combination of tomographic ultrasound imaging and three-dimensional magnetic resonance imaging-based model to diagnose postpartum levator avulsion. Scientific Reports, 2017, 7, 11235.	3.3	15
42	Low-frequency ultrasound-induced VEGF suppression and synergy with dendritic cell-mediated anti-tumor immunity in murine prostate cancer cells in vitro. Scientific Reports, 2017, 7, 5778.	3.3	17
43	Preliminary study of confounding factors of elastography and the application of fine-needle aspiration in thyroid nodules with indeterminate elastography. Scientific Reports, 2017, 7, 18005.	3.3	3
44	Phase-transitional Fe ₃ O ₄ /perfluorohexane Microspheres for Magnetic Droplet Vaporization. Theranostics, 2017, 7, 846-854.	10.0	26
45	Role of real-time elastography in assessing the stage of thrombus. International Angiology, 2017, 36, 59-63.	0.9	12
46	Contrast-enhanced ultrasound evaluation of pancreatic cancer xenografts in nude mice after irradiation with sub-threshold focused ultrasound for tumor ablation. Oncotarget, 2017, 8, 37584-37593.	1.8	1
47	Efficacy of sub-threshold focused ultrasound irradiation against pancreatic cancer xenografts evaluated using magnetic resonance imaging. Oncotarget, 2017, 8, 80453-80460.	1.8	3
48	MiR-491-5p negatively regulates cell proliferation and motility by targeting PDGFRA in prostate cancer. American Journal of Cancer Research, 2017, 7, 2545-2553.	1.4	21
49	Upregulation of ULK1 expression in PC-3 cells following tumor protein P53 transfection by sonoporation. Oncology Letters, 2016, 11, 699-704.	1.8	9
50	Study on the use of quantitative ultrasound evaluation of diabetic neuropathy in the rat sciatic nerve. Australasian Physical and Engineering Sciences in Medicine, 2016, 39, 997-1005.	1.3	7
51	Low-frequency ultrasound-mediated microvessel disruption combined with docetaxel to treat prostate carcinoma xenografts in nude mice: A novel type of chemoembolization. Oncology Letters, 2016, 12, 1011-1018.	1.8	11
52	Clinical Relevance of Left Atrial Strain to Predict Recurrence of Atrial Fibrillation after Catheter Ablation: A Metaâ€Analysis. Echocardiography, 2016, 33, 724-733.	0.9	40
53	Contrast-Enhanced Ultrasonography with Quantitative Analysis allows Differentiation of Renal Tumor Histotypes. Scientific Reports, 2016, 6, 35081.	3.3	36
54	Theranostic hollow/mesoporous organosilica nanospheres enhance the therapeutic efficacy of anticancer drugs in metastatic hormone-resistant prostate cancer. RSC Advances, 2016, 6, 94058-94067.	3.6	10

#	Article	IF	CITATIONS
55	Quantitative Study of Elasticity of Rabbit VX2 Liver Tumor with Alternated Cooling and Heating Treatment based on ARFI Ultrasound Imaging Technique. Scientific Reports, 2016, 6, 29303.	3.3	3
56	Liposome-mediated transfection of wild-type P53 DNA into human prostate cancer cells is improved by low-frequency ultrasound combined with microbubbles. Oncology Letters, 2016, 11, 3829-3834.	1.8	13
57	Diagnostic value of contrast-enhanced ultrasound in solid thyroid nodules with and without enhancement. Endocrine, 2016, 53, 480-488.	2.3	41
58	Papillary thyroid microcarcinoma co-exists with Hashimoto's thyroiditis: Is strain elastography still useful?. Ultrasonics, 2016, 68, 127-133.	3.9	6
59	Re: Tumor size measured by preoperative ultrasonography and postoperative pathologic examination in papillary thyroid carcinoma: relative differences according to size, calcification and coexisting thyroiditis. European Archives of Oto-Rhino-Laryngology, 2016, 273, 791-792.	1.6	0
60	Optimization of low-frequency low-intensity ultrasound-mediated microvessel disruption on prostate cancer xenografts in nude mice using an orthogonal experimental design. Oncology Letters, 2015, 10, 2999-3007.	1.8	11
61	Low-frequency and low-intensity ultrasound-mediated microvessel disruption enhance the effects of radiofrequency ablation on prostate cancer xenografts in nude mice. Molecular Medicine Reports, 2015, 12, 7517-7525.	2.4	7
62	Upregulation of Beclin-1 expression in DU-145 cells following low-frequency ultrasound irradiation combined with microbubbles. Oncology Letters, 2015, 10, 2487-2490.	1.8	5
63	3-Tesla magnetic resonance imaging improves the prostate cancer detection rate in transrectral ultrasound-guided biopsy. Experimental and Therapeutic Medicine, 2015, 9, 207-212.	1.8	9
64	Microscopic study of ultrasound–mediated microbubble destruction effects on vascular smooth muscle cells. Asian Pacific Journal of Tropical Medicine, 2015, 8, 325-329.	0.8	2
65	Diagnostic performance of the automated breast volume scanner: a systematic review of inter-rater reliability/agreement and meta-analysis of diagnostic accuracy for differentiating benign and malignant breast lesions. European Radiology, 2015, 25, 3638-3647.	4.5	34
66	Transforming Growth Factor β1 Could Influence Thyroid Nodule Elasticity and Also Improve Cervical Lymph Node Metastasis in Papillary Thyroid Carcinoma. Ultrasound in Medicine and Biology, 2015, 41, 2866-2872.	1.5	7
67	Transrectal real-time elastography-guided transperineal prostate biopsy as an improved tool for prostate cancer diagnosis. International Journal of Clinical and Experimental Medicine, 2015, 8, 6522-9.	1.3	9
68	Three-dimensional Ultrasound Appearance of Pelvic Floor in Nulliparous Women and Postpartum Women One Week after Their First Delivery. International Journal of Medical Sciences, 2014, 11, 234-239.	2.5	9
69	Caveolin-1 as a biomarker to predict therapeutic effect of low-frequency ultrasound combined with SonoVue on prostate cancer in nude mice model. Cancer Biomarkers, 2014, 14, 279-286.	1.7	1
70	Inhibitory effects of subcutaneous tumors in nude mice mediated by low-frequency ultrasound and microbubbles. Oncology Letters, 2014, 7, 1385-1390.	1.8	12
71	Enhanced antitumor effects of low-frequency ultrasound and microbubbles in combination with simvastatin by downregulating caveolin-1 in prostatic DU145 cells. Oncology Letters, 2014, 7, 2142-2148.	1.8	8
72	Facilitated brain delivery of poly (ethylene glycol)–poly (lactic acid) nanoparticles by microbubble-enhanced unfocused ultrasound. Biomaterials, 2014, 35, 3384-3395.	11.4	49

#	Article	IF	CITATIONS
73	Assessment of alternated cooling and heating treatment by US combined CEUS in the VX2 rabbit liver tumor model. Science Bulletin, 2014, 59, 865-873.	1.7	1
74	Combined treatment of PC-3 cells with ultrasound and microbubbles suppresses invasion and migration. Oncology Letters, 2014, 8, 1372-1376.	1.8	7
75	Low-frequency low energy ultrasound combined with microbubbles induces distinct apoptosis of A7r5 cells. Molecular Medicine Reports, 2014, 10, 3282-3288.	2.4	12
76	MicroPure Imaging for the Evaluation of Microcalcifications in Gouty Arthritis Involving the First Metatarsophalangeal Joint: A Preliminary Study. PLoS ONE, 2014, 9, e95743.	2.5	11
77	Treatment of PC-3 cells with ultrasound combined with microbubbles induces distinct alterations in the expression of Bcl-2 and Bax. Science Bulletin, 2013, 58, 3535-3540.	1.7	3
78	Contrast-enhanced ultrasound versus conventional ultrasound in the diagnosis of polypoid lesion of gallbladder: A multi-center study of dynamic microvascularization. Clinical Hemorheology and Microcirculation, 2013, 55, 359-374.	1.7	30
79	Radiation force calculation and acoustic power measurement for a cylindrical concave transducer based on the ray acoustic model. Journal of the Korean Physical Society, 2012, 61, 544-550.	0.7	2
80	Induction of the apoptosis of cancer cell by sonodynamic therapy: a review. Chinese Journal of Cancer Research: Official Journal of China Anti-Cancer Association, Beijing Institute for Cancer Research, 2012, 24, 368-373.	2.2	52
81	Experiment on building a real-time temperature field distribution model of the prostate using special data encryption multi-pole radiofrequency ablation and a visualization phantom. Science Bulletin, 2011, 56, 3845-3853.	1.7	1
82	Assessment of levator hiatus by 3D ultrasound volume contrast imaging in normal nulliparas. Journal of Shanghai Jiaotong University (Science), 2009, 14, 371-375.	0.9	0